

Thiophene Methanimine–Palladium Schiff Base Complex Anchored on Magnetic Nanoparticles: A Novel, Highly Efficient and Recoverable Nanocatalyst for Cross-Coupling Reactions in Mild and Aqueous Media

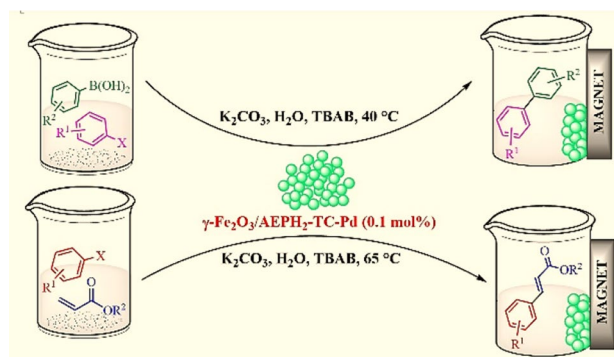
γ -Fe₂O₃/AEPH₂-TC-Pd Catalyzed Suzuki–Miyaura and Heck–Mizoroki Reactions

Roya Jahanshahi¹ · Batool Akhlaghinia¹

Received: 8 June 2017 / Accepted: 14 August 2017 / Published online: 28 August 2017
© Springer Science+Business Media, LLC 2017

Abstract In this study, a novel thiophene methanimine–palladium Schiff base complex anchored on decorated γ -Fe₂O₃ with 2-aminoethyl dihydrogen phosphate (γ -Fe₂O₃/AEPH₂-TC-Pd) was synthesized as a new magnetically separable nanocatalyst. Characterization of the new designed nanocatalyst was performed successfully using different techniques such as FT-IR, XRD, XPS, TEM, TGA, VSM, ICP and elemental analysis. This nanocatalyst presented a superb catalytic activity for Suzuki–Miyaura and Heck–Mizoroki cross-coupling reactions. The most important features of the prepared catalytic system which makes the current protocol more beneficial from both industrial and environmental viewpoints are its ease of recovery and reusability up to nine cycles without appreciable loss of the catalytic performance, as well as accomplishing the reactions under mild conditions in aqueous media which is a great challenge in some cross-coupling reactions.

Graphical Abstract



Keywords γ -Fe₂O₃/AEPH₂-TC-Pd · Sustainable chemistry · Magnetically separable nanocatalyst · Palladium–Schiff base complex · Suzuki–Miyaura · Heck–Mizoroki

1 Introduction

Nowadays, novel approaches focus on development of more environmentally sustainable chemical processes in both academic and industrial viewpoints [1]. One of the important criteria that support a chemical transformation in a movement toward the green chemistry, is utilizing the heterogeneous catalytic systems instead of their homogeneous counterparts [2, 3]. Although homogeneous catalysts provide excellent activity and selectivity, they are encounter with the problems associated with catalyst separation, catalyst recycling and the contamination of the ligand or metal residue in the final products [4]. On the other hand, in spite of having substantial merits in terms of stability and reusability, heterogeneous catalysts have lower activity and selectivity

Electronic supplementary material The online version of this article (doi:10.1007/s10562-017-2170-x) contains supplementary material, which is available to authorized users.

✉ Batool Akhlaghinia
akhlaghinia@um.ac.ir

¹ Department of Chemistry, Faculty of Sciences, Ferdowsi University of Mashhad, Mashhad 9177948974, Iran

compared with homogeneous catalytic systems, which is due to their lower available surface area [5]. Interestingly, the combination of nanotechnology and heterogeneous catalytic systems through the immobilization of the stable ligands, complexes and other catalytic species onto the nanostructured supports, could overcome the mentioned drawbacks [5, 6]. In the other words, nano-chemical technology has closed the homogeneous and heterogeneous catalytic systems from activity and selectivity outlooks.

Among various nanostructured supports, magnetic nanoparticles (MNPs) have emerged as one of the most popular ones [7]. The main advantage of MNPs is that they can be easily separated from the reaction media by applying a simple external magnetic field without using traditional filtration or centrifugation approaches. Additionally, MNPs have superlative physical properties such as excellent chemical and thermal stability, high surface area and the surface modification ability [8].

Suzuki–Miyaura and Heck–Mizoroki cross-coupling reactions are one of the most potent transformations for the effective and straightforward C–C bond formation. The resulting coupling products have extensive applications as fundamental building blocks in the synthesis of numerous structurally diverse molecules in several fields of the chemistry such as pharmaceuticals, agrochemicals and material sciences [9–11]. General driving force to furnish such a beneficial transformation is the transition metal-catalyzed cross-coupling reactions [12, 13]. Among various transition metals [14], palladium has been the first choice and is still considered as one of the most commonly investigated metals for cross-coupling reactions [15–18]. Traditionally, Suzuki–Miyaura and Heck–Mizoroki cross-coupling reactions were performed under homogeneous palladium catalytic systems comprising various ligands such as *N*-heterocyclic carbenes [19], dibenzylideneacetone (dba) [20], phosphines [9, 21, 22], thiols [23], phthalocyanines [24], palladacycles [25], porphyrins [26], imidazolium [27] and Schiff bases [28]. Although, each of these approaches has their own advantages, but they suffer from previously mentioned limitations related to the homogeneous catalytic systems. By consideration the above facts, designing the heterogeneous Pd-based catalysts *via* the immobilization of related palladium containing catalysts on different supports [29–36] has recently gathered a great deal of attention.

A well-known strategy for preparing a heterogeneous catalyst is anchoring a suitable ligand to a support surface for further immobilization of a transition metal [37, 38]. The selected ligand for this purpose has a vital influence on tuning the catalyst activity and catalyst stability at room temperature in air or in aqueous solution [39]. Using a proper support or supported ligand for Pd heterogenization would offer a stable and reusable catalytic system with the minimized metal leaching and aggregation issues [40, 41].

2-Aminoethyl dihydrogen phosphate (AEPH₂) is a type of an almost unknown biodegradable phospholipidic compound, which has very recently attracted an increasing attention as a surface modification ligand [5, 42–47].

In spite of a great deal of heterogeneous catalytic systems suggested for Suzuki–Miyaura and Heck–Mizoroki cross-coupling reactions to date, furnishing such a reactions in aqueous and also mild conditions is still an essential requirement, especially for more challenging partners due to the performance of side reactions in Suzuki–Miyaura cross-coupling reactions and inherent difficulty of Heck–Mizoroki cross-coupling reactions under mild conditions.

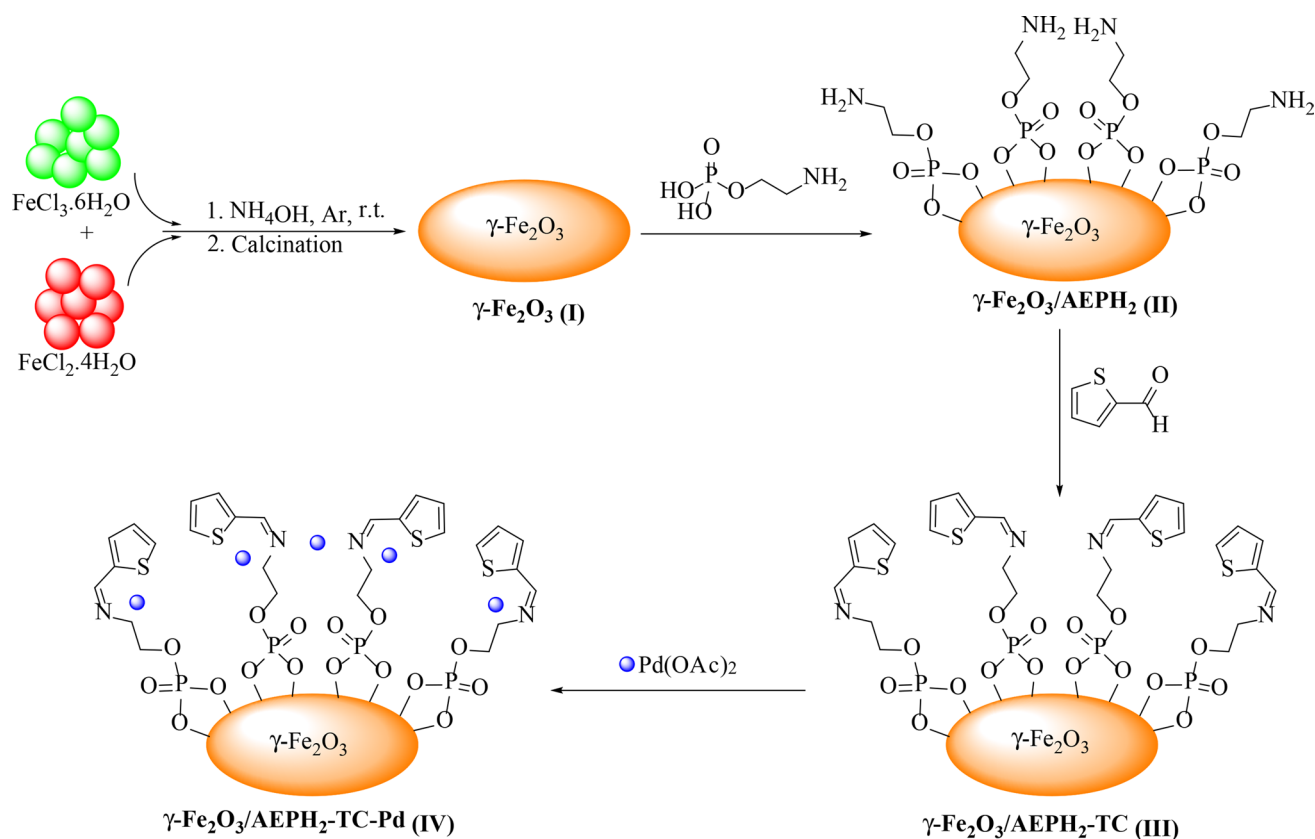
Considering the above facts and as a part of our ongoing research interest in developing new heterogeneous catalysts [43–54], herein, we have synthesized a novel thiophene methanimine-palladium Schiff base complex anchored on decorated γ -Fe₂O₃ with 2-aminoethyl dihydrogen phosphate (γ -Fe₂O₃/AEPH₂-TC-Pd) as a highly efficient magnetically separable nanocatalyst (Scheme 1). We hoped to conduct these coupling reactions upon mild and aqueous media by means of the existence of nitrogen and sulfur containing ligand in the catalyst structure, which can strongly stabilized the palladium species. The catalytic activity of γ -Fe₂O₃/AEPH₂-TC-Pd was subsequently investigated towards the Suzuki–Miyaura and Heck–Mizoroki cross-coupling reactions, in green media (see Scheme 2 and 3). The proposed catalytic system has privileged features such as high stability, moisture and air insensitiveness as well as satisfying magnetic separability along with simple catalytic preparation procedure.

2 Experimental

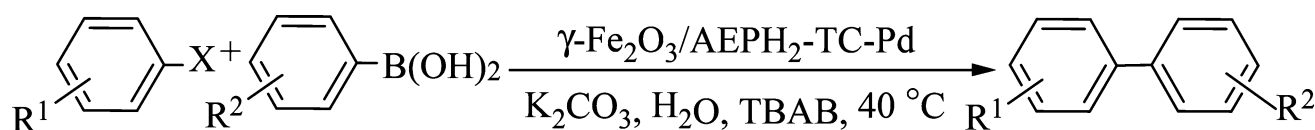
2.1 Materials and Instruments

All chemical reagents and solvents were purchased from Merck and Sigma-Aldrich chemical companies and were used as received without further purification. γ -Fe₂O₃ nanoparticles were prepared by the previously reported chemical co-precipitation technique in literature [55].

The purity determinations of the products and the progress of the reactions were accomplished by TLC on silica gel polygram STL G/UV 254 plates. The melting points of the products were determined with an Electrothermal Type 9100 melting point apparatus. The FT-IR spectra were recorded on pressed KBr pellets using an AVATAR 370 FT-IR spectrometer (Therma Nicolet spectrometer, USA) at room temperature in the range between 4000 and 400 cm⁻¹ with a resolution of 4 cm⁻¹. The NMR spectra were provided by Bruker Avance 300, 400 and 500 MHz instruments in CDCl₃ in the presence of tetramethylsilane as the internal standard and the coupling constants (*J* values)



Scheme 1 An overview on the synthesis of $\gamma\text{-Fe}_2\text{O}_3/\text{AEPH}_2\text{-TC-Pd}$ nanocatalyst



$\text{R}^1 = \text{Ph}, 4\text{-NO}_2\text{C}_6\text{H}_4, 4\text{-ClC}_6\text{H}_4, 4\text{-OMeC}_6\text{H}_4, 4\text{-MeC}_6\text{H}_4, 2\text{-Me-4-NO}_2\text{C}_6\text{H}_3,$
 $3\text{-CHOC}_6\text{H}_4, 4\text{-CHOC}_6\text{H}_4, 4\text{-CNC}_6\text{H}_4, 2\text{-Thiophene}$

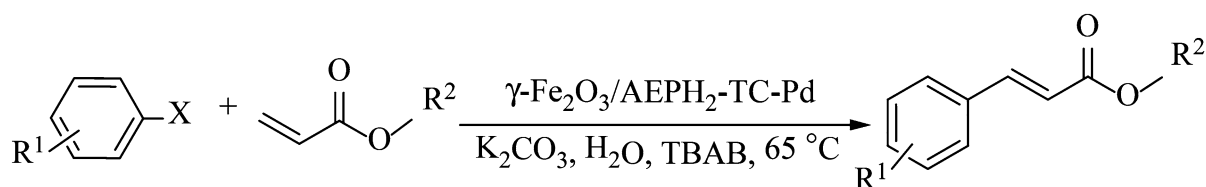
$\text{R}^2 = \text{H}, 3\text{-NO}_2$

$\text{X} = \text{I, Br, Cl, F}$

Scheme 2 Suzuki–Miyaura cross-coupling reaction in the presence of $\gamma\text{-Fe}_2\text{O}_3/\text{AEPH}_2\text{-TC-Pd}$ nanocatalyst

are given in Hz. Elemental analyses were performed using a Thermo Finnigan Flash EA 1112 Series instrument (furnace: 900 °C, oven: 65 °C, flow carrier: 140 mL min⁻¹, flow reference: 100 mL min⁻¹). Mass spectra were recorded with a CH7A Varianmat Bremem instrument at 70 eV electron impact ionization, in *m/z* (rel%). Thermogravimetric analysis (TGA) was carried out using a Shimadzu Thermogravimetric Analyzer (TG-50) in the temperature range

of 25–900 °C at a heating rate of 10 °C min⁻¹, under air atmosphere. Transmission electron microscopy (TEM) was performed with a Leo 912 AB microscope (Zeiss, Germany) with an accelerating voltage of 120 kV. Room temperature magnetization isotherms were obtained using a vibrating sample magnetometer (VSM) (Magnetic DaneshPajoh Inst.). Inductively coupled plasma optical emission spectroscopy (ICP-OES) was carried out on a 76004555 SPECTRO



$R^1 = \text{Ph}, 4\text{-NO}_2\text{C}_6\text{H}_4, 4\text{-ClC}_6\text{H}_4, 4\text{-OMeC}_6\text{H}_4, 4\text{-MeC}_6\text{H}_4, 4\text{-CNC}_6\text{H}_4, 4\text{-CHOC}_6\text{H}_4, 2\text{-Thiophene}$

$R^2 = \text{Me}, \text{Bu}^n$

$X = \text{I}, \text{Br}, \text{Cl}$

Scheme 3 Heck–Mizoroki cross-coupling reaction in the presence of $\gamma\text{-Fe}_2\text{O}_3/\text{AEPH}_2\text{-TC-Pd}$ nanocatalyst

ARCOS ICP-OES analyzer. The crystal structure of the catalyst was analyzed by XRD using a D8 ADVANCE-Bruker diffractometer operated at 40 kV and 30 mA, utilizing Cu $K\alpha$ radiation ($\lambda = 0.154 \text{ \AA}$), at a step size of 0.040° and step time of 1.5 s. X-ray photoelectron spectroscopy (XPS) was performed using the Thermo Scientifi, ESCALAB 250 Xi Mg X-ray resource. All yields refer to isolated products after purification by thin layer chromatography. In addition, all of the products were known compounds and they were characterized by ^1H NMR, ^{13}C NMR spectroscopy, and mass spectrometry and comparison of their melting points with known compounds.

2.2 Preparation of $\gamma\text{-Fe}_2\text{O}_3$ Nanoparticles (I)

$\text{FeCl}_2 \cdot 4\text{H}_2\text{O}$ (0.01 mol, 1.99 g) and $\text{FeCl}_3 \cdot 6\text{H}_2\text{O}$ (0.01 mol, 3.25 g) with a mole ratio of 1:1, were dissolved in deionized water (30 mL) under argon atmosphere at room temperature. A NH_4OH solution (0.6 M, 200 mL) was then added drop by drop (drop rate = 1 mL min^{-1}) into the stirring mixture at room temperature. When the reaction pH was reached to 11, addition of NH_4OH solution was stopped. The resulting black dispersion was vigorously stirred for 1 h at room temperature, followed by heating to reflux temperature for 1 h to yield a brown dispersion. The resultant magnetic nanoparticles were next separated using a magnetic bar, washed with deionized water ($5 \times 20 \text{ mL}$) and then dried at 40°C for 24 h. Thereafter, the obtained nanoparticles were heated at 2°C min^{-1} up to 220°C , and then kept in the furnace for 3 h to give a reddish-brown powder.

2.3 Preparation of $\gamma\text{-Fe}_2\text{O}_3$ NPs Functionalized with AEPH₂ ($\gamma\text{-Fe}_2\text{O}_3/\text{AEPH}_2$) (II)

$\gamma\text{-Fe}_2\text{O}_3$ nanoparticles (1 g) were dispersed in 20 mL deionized water by sonication for 20 min. Then, AEPH₂ (0.7 g, 5 mmol) was added portion by portion to the resulting suspension and the obtained mixture was vigorously stirred at room temperature. After 12 h, the afforded material

($\gamma\text{-Fe}_2\text{O}_3/\text{AEPH}_2$) (II) was separated by an external magnet, washed with distilled water repeatedly and air-dried.

2.4 Preparation of $\gamma\text{-Fe}_2\text{O}_3/\text{AEPH}_2\text{-TC}$ (III)

1 g of $\gamma\text{-Fe}_2\text{O}_3/\text{AEPH}_2$ (II) was dispersed in dried methanol (20 mL), by placing in an ultrasonic bath for 20 min. Thereupon, thiophene-2-carbaldehyde (TC) (0.8 g) was added to the resulting suspension, followed by refluxing for 4 h. In the last step, the obtained nanoparticles were separated by magnetic decantation and repeatedly washed with hot ethanol and finally dried at ambient temperature overnight.

2.5 Preparation of $\gamma\text{-Fe}_2\text{O}_3/\text{AEPH}_2\text{-TC-Pd}$ (IV)

The prepared $\gamma\text{-Fe}_2\text{O}_3/\text{AEPH}_2\text{-TC}$ (1 g) was sonicated in ethanol (30 mL) for 30 min. After that, a solution of $\text{Pd}(\text{OAc})_2$ (0.34 mmol, 0.076 g) in ethanol (10 mL) was added to the dispersed suspension and continuous stirring was conducted at reflux condition for 12 h. After cooling down to room temperature, the solid nanocatalyst was separated from the reaction medium using an external magnet. The nanocatalyst preparation process was completed by washing the resultant material with ethanol ($3 \times 15 \text{ mL}$) before being dried under vacuum at 50°C .

2.6 Typical Procedure for Suzuki–Miyaura Cross-Coupling Reaction

Typically, a 10-mL round-bottom flask was charged with iodobenzene (1.0 mmol, 0.204 g), phenylboronic acid (1.1 mmol, 0.134 g), K_2CO_3 (1.2 mmol, 0.165 g), TBAB (0.2 mmol, 0.064 g), H_2O (3 mL) and 0.0015 g of $\gamma\text{-Fe}_2\text{O}_3/\text{AEPH}_2\text{-TC-Pd}$ (0.1 mol%). The resultant mixture was heated under stirring at 40°C for 10 min. After completion of the reaction (as judged by TLC), the reaction mixture was allowed to cool down to room temperature and the nanocatalyst was easily separated by using a proper magnetic field, washed with EtOH and vacuum-dried at 50°C to be ready

for utilizing in successive runs. Subsequently, the reaction mixture was extracted with ethyl acetate (5 × 5 mL). Combined organic phase was dried over anhydrous Na₂SO₄, and solvent was next removed on a rotary evaporator. Thereafter, the obtained crude product was chromatographed on silica gel (eluted with *n*-hexane:ethyl acetate; 50:1), to afford the corresponding pure product (0.148 g, % 98 yield).

2.7 Typical Procedure for Heck–Mizoroki Coupling Reaction

Typically, a 10-mL round-bottom flask was charged with iodobenzene (1.0 mmol, 0.204 g), *n*-butyl acrylate (1.1 mmol, 0.140 g), K₂CO₃ (1.2 mmol, 0.165 g), TBAB (0.2 mmol, 0.064 g), H₂O (3 mL) and 0.0015 g of γ -Fe₂O₃/AEPH₂-TC-Pd (0.1 mol%). The resulting mixture was heated under stirring at 65 °C till the reaction was judged to be complete by TLC (10 min). Then, the reaction mixture was allowed to cool down to room temperature and the nanocatalyst was easily separated by using a proper magnetic field, washed with EtOH and vacuum-dried at 50 °C to be ready for utilizing in the next run. Thereupon, the reaction mixture was extracted with ethyl acetate (5 × 5 mL). Combined organic phase was dried over anhydrous Na₂SO₄, and solvent was then removed on a rotary evaporator. Afterwards, the obtained crude product was chromatographed on silica gel (eluted with *n*-hexane:ethyl acetate; 50:1), to afford the corresponding pure product (0.148 g, % 98 yield).

3 Results and Discussion

γ -Fe₂O₃/AEPH₂-TC-Pd as a new heterogeneous nanocatalyst was synthesized according to the pathway shown in Scheme 1.

It is important to note that the stability of the phosphonate linker which has utilized for fabrication of the respective nanocatalyst, as well as the simplicity of its tethering on the magnetic γ -Fe₂O₃ support [56], besides its ability to act as stabilizing palladium agent against agglomeration and palladium black formation, makes the presented protocol more fascinating.

3.1 Characterization of γ -Fe₂O₃/AEPH₂-TC-Pd

FT-IR spectroscopy was conducted for every step of the nanocatalyst synthesis to verify the successful functionalization of the MNPs surface (Fig. 1). As it is exhibited in Fig. 1a, the absorption bands at around 698–571 cm⁻¹ are attributed to the vibration of Fe–O bonds in the crystalline lattice of γ -Fe₂O₃ [57]. The characteristic bands at 3436 and 1620 cm⁻¹ are respectively ascribed to the stretching and bending vibration modes of the surface attached

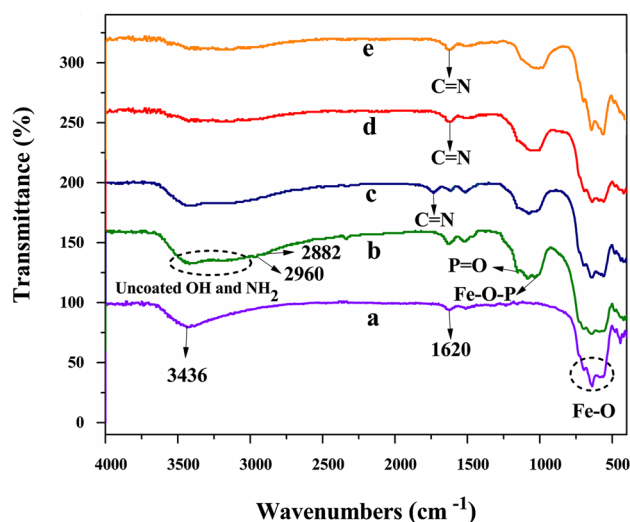


Fig. 1 FT-IR spectra of *a* γ -Fe₂O₃; *b* γ -Fe₂O₃/AEPH₂; *c* γ -Fe₂O₃/AEPH₂-TC; *d* γ -Fe₂O₃/AEPH₂-TC-Pd and *e* 9th recovered γ -Fe₂O₃/AEPH₂-TC-Pd

hydroxyl groups and adsorbed water molecules [58, 59]. In the FT-IR spectrum of γ -Fe₂O₃/AEPH₂ (Fig. 1b), the appearance of the broad absorption band in the region of about 3600–3000 cm⁻¹, could be related to the overlapping of uncoated O–H and NH₂ stretching modes [5]. Moreover, the absorption bands visualized at 2960 and 2882 cm⁻¹, could be in turn assigned to the asymmetric and symmetric methylene C–H stretching vibrational frequencies [60]. Also, the stretching vibrations of P=O and Fe–O–P bonds which were observed at 1150 and 1030 cm⁻¹, respectively [5], would confirm the successful chemical attachment of AEPH₂ onto the MNPs surface. Schiff base formation was verified by the appearance of characteristic absorption band of imine group (C=N) at 1656 cm⁻¹ [61], as well as the intensity diminution of NH₂ stretching band (Fig. 1c). It is interesting to note that upon metallation with palladium acetate, the diagnostic absorption band of C=N bond at 1656 cm⁻¹ was shifted to a lower wave number (1640 cm⁻¹) [62]. These results confirmed the strong metal–ligand interaction (Fig. 1d).

Furthermore, XRD analysis was conducted to perceive the crystalline nature of the novel synthesized catalyst (Fig. 2). As it is obvious in the XRD pattern of γ -Fe₂O₃/AEPH₂-TC-Pd, the presence of characteristic peaks appeared at angles attributing to (2 2 0), (3 1 1), (4 0 0), (4 2 2), (5 1 1) and (4 4 0) reflection planes are in a good agreement with the face-centered cubic structure of γ -Fe₂O₃ (JCPDS file no. 01-078-6916) [63, 64]. Importantly, three diffraction peaks appeared at 2 θ = 40.00, 46.40 and 68.06 corresponding to (1 1 1), (2 0 0) and (2 2 0) crystallographic planes, respectively, could be assigned to the existence of the face-centered cubic structure of Pd(0) (JCPDS file no.

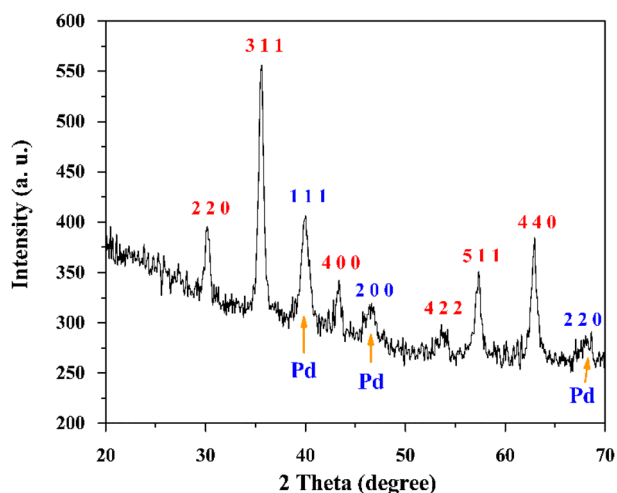


Fig. 2 XRD pattern of γ -Fe₂O₃/AEPH₂-TC-Pd

05-0681) in the nanocatalyst structure [65, 66]. The average crystallite size of γ -Fe₂O₃ nanoparticles (15 nm), which was calculated using Debye–Scherrer equation, is well matched

with the average particle size observed in the TEM analysis (See Figs. 4, 5).

X-ray photoelectron spectroscopy (XPS) is a powerful technique to evaluate the electron properties of the species anchored on the surface, such as oxidation state, electron environment and the binding energy of the core electron of the metal. As can be seen in the XPS spectra of both fresh γ -Fe₂O₃/AEPH₂-TC-Pd and ninth reused nanocatalyst (Fig. 3a, b), the presence of binding energies at 335.0 and 335.1 eV (due to Pd 3d_{5/2}) alongside the binding energies at 340.2 and 340.3 eV (due to Pd 3d_{3/2}) relating in turn to the fresh and ninth reused nanocatalyst, might be assigned to the metallic Pd with zero oxidation state [67, 68]. Moreover, the peaks corresponding to P, C, N, O, Fe and Pd atoms are also clearly observed in the XPS elemental survey of both fresh and ninth reused nanocatalyst (Fig. 3c, d).

The XPS analysis in agreement with XRD pattern, contributes to the presence of metallic Pd nanoparticles in the prepared catalyst, while we used no reducing agent during the immobilization of Pd species. Construction of metallic Pd nanoparticles in our designed catalyst could be attributed to the presence of thiophene rings and some

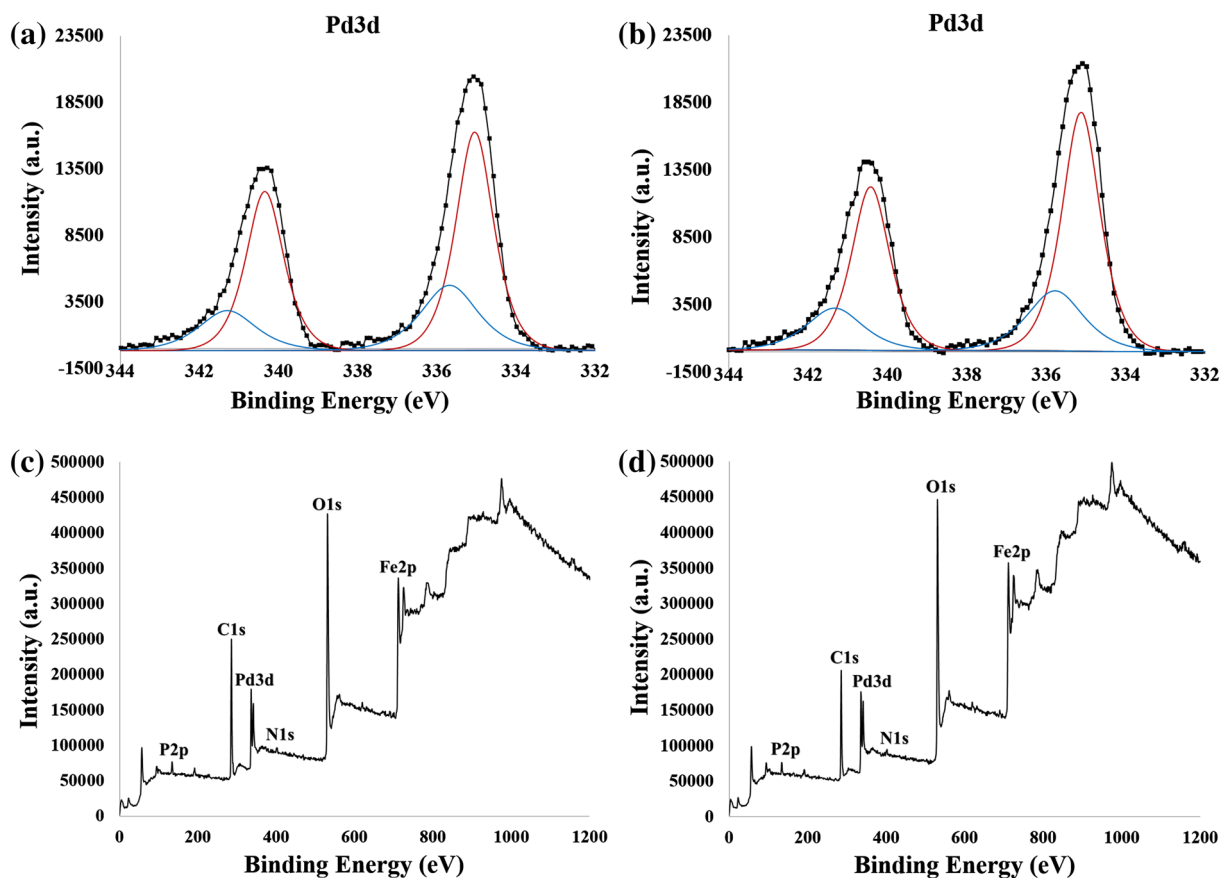


Fig. 3 XPS spectra of the fresh and 9th recovered γ -Fe₂O₃/AEPH₂-TC-Pd showing Pd 3d_{5/2} and Pd 3d_{3/2} binding energies (a, b) and XPS elemental survey scan of the fresh and 9th recovered nanocatalyst (c, d)

Fig. 4 TEM images of γ -Fe₂O₃/AEPH₂-TC-Pd

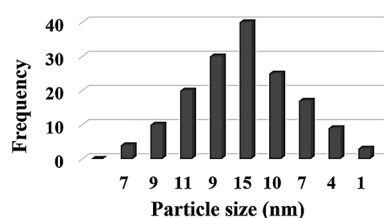
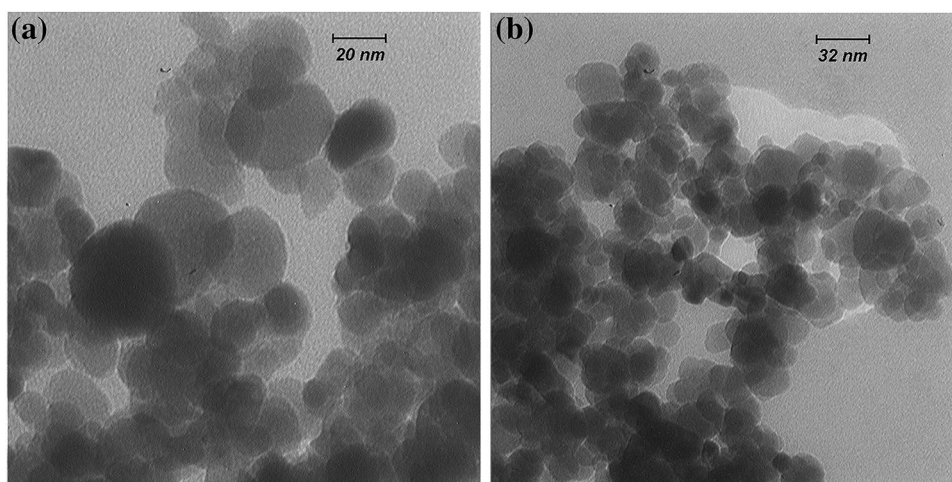


Fig. 5 Particle size distribution histogram of γ -Fe₂O₃/AEPH₂-TC-Pd

existing heteroatoms on the structure of the catalyst, which can increase the electron density of the support surface. On the other hand, ethanol also can operate as a reducing agent during the synthetic procedure.

TEM images of the new nanocatalyst were recorded and shown in Fig. 4. It can be easily deduced from TEM images that the as-synthesized catalyst has spherical morphology with a very satisfying monodispersity. Particle size distribution of γ -Fe₂O₃/AEPH₂-TC-Pd which was calculated according to the TEM analysis displayed that the average diameter of the nanoparticles are about 15 nm (Fig. 5).

TGA was carried out to determine the thermal stability and organic content of the new nanocatalyst (Fig. 6). The obtained results revealed two significant mass changes at different temperature ranges. The first mass change of about 1.9% below 200 °C, could be assigned to remove of the trapped physically adsorbed water and probably ethanol. The second and indeed the significant mass change, which was started at around 200 °C and continued up to 670 °C can be attributed to the elimination of organic functional groups incorporated in the surface of γ -Fe₂O₃ MNPs (15.5%). According to the TGA, the amount of organic motif supported on γ -Fe₂O₃ MNPs was estimated to be 0.85 mmol g⁻¹. These findings were in a very good agreement with the obtained elemental analysis data (N = 1.2% and C = 5.62%) and ICP-OES, as well. The ICP-OES analysis of γ -Fe₂O₃/

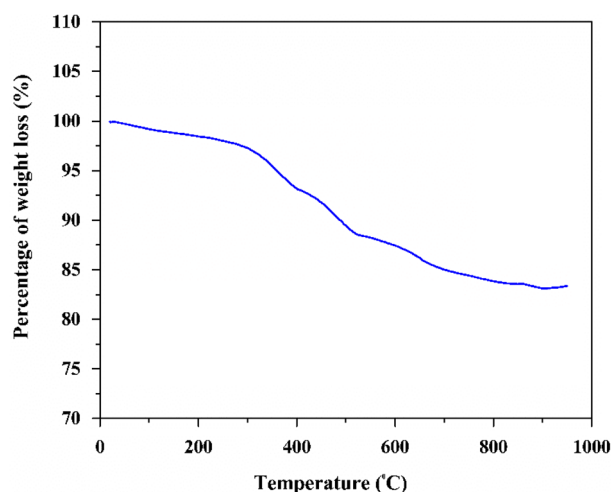


Fig. 6 TGA thermogram of γ -Fe₂O₃/AEPH₂-TC-Pd

AEPH₂-TC-Pd represented that 0.87 mmol of palladium was anchored on 1.00 g of the nanocatalyst.

Magnetic behavior of the novel synthesized nanocatalyst in comparison with bare γ -Fe₂O₃ MNPs was evaluated, using VSM analysis (Fig. 7). As it is evident from the resulting magnetization curves, the value of saturation magnetic moment of the prepared nanocatalyst was diminished from 76 to 60 emu g⁻¹. This reduction in the saturation magnetic moment arises from the surface modification of γ -Fe₂O₃ MNPs with non-magnetic materials during the catalyst synthetic pathway. By the way, having the superparamagnetic property, guarantees very facile and efficient separation of the nanocatalyst from the reaction media.

3.2 Heterogeneity Tests

To ascertain whether the catalyst is actually functioning in a heterogeneous pathway or not, a variety of different control

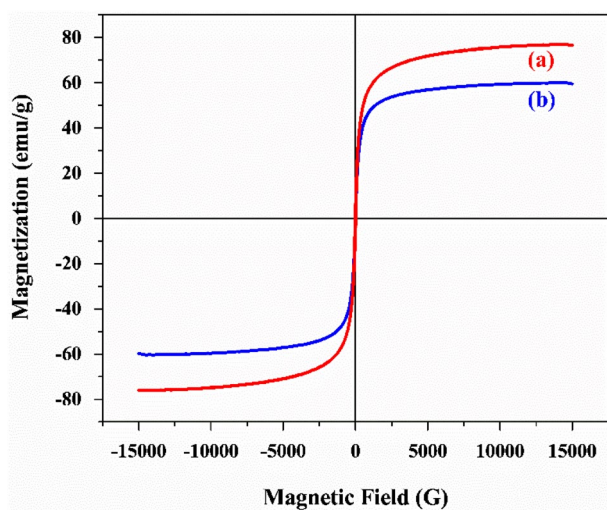


Fig. 7 Magnetization curves of *a* γ - Fe_2O_3 and *b* γ - $\text{Fe}_2\text{O}_3/\text{AEPH}_2\text{-TC-Pd}$

experiments have been performed. Firstly, we conducted a hot-filtration test for the model Suzuki–Miyaura coupling reaction under the optimal conditions. In this line, precisely 10 min after the reaction starting (before complete consumption of all substrates), the catalyst was separated from the reaction mixture using an external magnet. In this step, only 45% conversion was achieved. Afterwards, the reaction was permitted to continue for further 3 h. No considerable reaction progress hereon, well suggested that no leaching of palladium happened during the reaction process. Nevertheless, a negative hot-filtration test could not be a conclusive indication for the actual catalytic activity attributed solely to heterogeneity [69]. This is due to the fact that in many circumstances the leached and soluble Pd species could be redepositing back on the insoluble support during the hot filtration. Hence, while the negative hot-filtration test might point out that the catalyst could be to some extent recyclable, it should not be considered as a unique evidence for heterogeneity of the solid catalysts [69].

To further clarify whether the γ - $\text{Fe}_2\text{O}_3/\text{AEPH}_2\text{-TC-Pd}$ -catalyzed cross-coupling reaction we encountered in this study is truly heterogeneous in nature or not, we also performed the typical poisoning test for the model Suzuki–Miyaura coupling reaction under the optimized conditions, using an excess amount of $\text{Hg}(0)$ (Hg/Pd , 400:1), as an effective palladium scavenger which selectively coordinates and deactivates the leached out palladium. In this regard, if the coupling reaction was proceeds through the leached out palladium species, the cessation of the reaction would be expected. However, affording the corresponding biphenyl in excellent isolated yield without any detectable induction period in this investigation, interestingly documented that no leaching of palladium takes

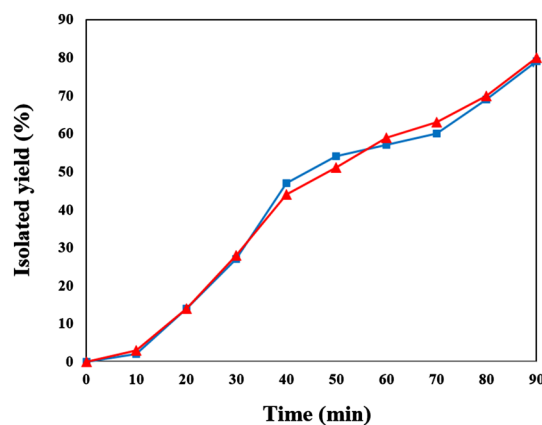


Fig. 8 Reaction progress as a function of time on the Suzuki–Miyaura cross-coupling reaction of 4-methoxy bromobenzene with phenylboronic acid by using γ - $\text{Fe}_2\text{O}_3/\text{AEPH}_2\text{-TC-Pd}$ catalyst in water under: normal conditions (red triangle); in the presence of 400 equivalents $\text{Hg}(0)$ (blue square)

place during the reaction and that the catalyst is purely heterogeneous in nature.

However, it is very essential to note that a negative result from the poisoning test by considering the final yield alone can sometimes consequence in an erroneous conclusion [70]. So, to further elucidate the heterogeneous nature of the designed nanocatalyst, we decided to set out some additional experiments to study the reaction kinetics, both in the absence and in the presence of the poison [$\text{Hg}(0)$ (Hg/Pd , 400:1)]. The kinetic experiments were conducted using 4-methoxy bromobenzene and phenylboronic acid as coupling partners under the optimized reaction conditions in the presence of γ - $\text{Fe}_2\text{O}_3/\text{AEPH}_2\text{-TC-Pd}$ (Fig. 8). In this study, the reaction progress was evaluated in 10-min intervals for both mentioned experiments. As it is obvious from data in Fig. 8, the reaction advancement was almost the same either in the absence or presence of the poison. So, based on the kinetic studies it could be nicely certified that the catalytic activity of the nanocatalyst derives from the leached out Pd. By considering all of the above investigations, we have speculated that the respective nanocatalyst most likely operated in a heterogeneous manner.

The heterogeneous pathway observed using this system might be attributed to the presence of sulfur-containing ligand on the surface of the catalyst. Since sulfur based ligands are strong Pd scavengers, we believed that the thiophene ligand on the structure of our catalyst is tightly reserved the Pd nanoparticles on the support surface and prevents their leaching to solution to act *via* possible homogeneous pathway.

3.3 Catalytic Activity of γ -Fe₂O₃/AEPH₂-TC-Pd in Suzuki–Miyaura Cross-Coupling Reaction

Following the successful preparation and characterization of γ -Fe₂O₃/AEPH₂-TC-Pd, to explore the potential activity of such a new heterogeneous nanocatalyst, its catalytic applicability was initially evaluated against the Suzuki–Miyaura cross-coupling reaction. In the preliminary assessment, the reaction conditions were optimized by varying the solvent, base, temperature and catalyst amount toward the model reaction of iodobenzene (1 mmol) with phenylboronic acid (1.1 mmol) (Table 1). When a blank experiment in the absence of catalyst was conducted by carrying out the model reaction in DMF at 100 °C, using 1:1.5 molar ratio of iodobenzene/K₂CO₃, only a trace amount of the product was acquired even after a prolonged time (Table 1, entry 1). Accordingly, the essential role of γ -Fe₂O₃/AEPH₂-TC-Pd

in the catalytic process of such a coupling reaction is highlighted. In the next step, to survey the influence of the solvent on the reaction progress, several solvents including DMF, CH₃CN, Toluene, EtOH, H₂O and H₂O/EtOH [1/1 (v/v)] were tested under the same conditions in the presence of 0.1 mol% of the catalyst (Table 1, entries 2–7). These experiments led us to found that H₂O and DMF were superior to all of the examined solvents. By the way, owing to the awful environmental impact of DMF, the conclusive choice for the reaction medium would be H₂O, especially regarding to the concepts of the green chemistry. Then, to assess the base effect on the reaction rate, a series of available bases were screened (Table 1, entries 8–12). As can be readily perceived from the data in Table 1, inorganic bases such as potassium carbonate (K₂CO₃), sodium hydrogen carbonate (NaHCO₃) and potassium hydroxide (KOH) were more effectual vs. the organic bases triethylamine, sodium acetate

Table 1 Suzuki–Miyaura cross-coupling reaction of iodobenzene with phenylboronic acid in the presence of γ -Fe₂O₃/AEPH₂-TC-Pd nanocatalyst, under different reaction conditions

Entry	Catalyst (mol%)	Molar ratios of iodobenzene:base	Base	Solvent	Additive (mmol)	Temp. (°C)	Time (min)	Isolated yield (%)
1	–	1:1.5	K ₂ CO ₃	DMF		100	18 h	Trace
2	0.1	1:1.5	K ₂ CO ₃	DMF		100	20	93
3	0.1	1:1.5	K ₂ CO ₃	CH ₃ CN		Reflux	60	25
4	0.1	1:1.5	K ₂ CO ₃	Toluene		Reflux	18 h	15
5	0.1	1:1.5	K ₂ CO ₃	EtOH		Reflux	20	82
6	0.1	1:1.5	K ₂ CO ₃	H ₂ O		100	20	91
7	0.1	1:1.5	K ₂ CO ₃	H ₂ O/EtOH 1/1		Reflux	35	90
8	0.1	1:1.5	Et ₃ N	H ₂ O		100	30	75
9	0.1	1:1.5	NaHCO ₃	H ₂ O		100	20	86
10	0.1	1:1.5	NaOAc	H ₂ O		100	60	36
11	0.1	1:1.5	KOH	H ₂ O		100	20	81
12	0.1	1:1.5	<i>n</i> -Butylamine	H ₂ O		100	4 h	25
13	0.1	1:1.5	K ₂ CO ₃	H ₂ O		80	25	85
14	0.1	1:1.2	K ₂ CO ₃	H ₂ O		80	25	85
15	0.1	1:1.1	K ₂ CO ₃	H ₂ O		80	45	79
16	0.1	1:2	K ₂ CO ₃	H ₂ O		80	25	85
17	0.09	1:1.2	K ₂ CO ₃	H ₂ O		80	60	82
18	0.1	1:1.2	K ₂ CO ₃	H ₂ O	TBAB ^a (0.2)	80	10	98
19	0.1	1:1.2	K ₂ CO ₃	H ₂ O	TBAB (0.2)	60	10	98
20	0.1	1:1.2	K ₂ CO ₃	H ₂ O	TBAB (0.2)	40	10	98
21	0.1	1:1.2	K ₂ CO ₃	H ₂ O	CTAB ^b (0.2)	40	15	64
22	0.1	1:1.2	K ₂ CO ₃	H ₂ O	SDS ^c (0.2)	40	15	35
23	0.1	1:1.2	K ₂ CO ₃	H ₂ O	TBAB (0.1)	40	35	87
24 ^d	0.1	1:1.2	K ₂ CO ₃	H ₂ O	TBAB (0.2)	40	2 h	15

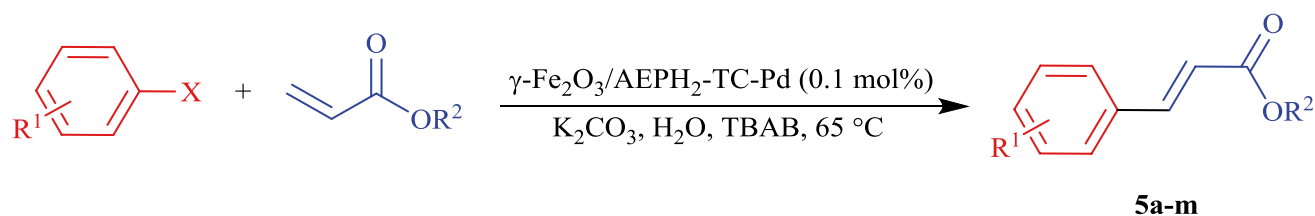
Reaction conditions: iodobenzene (1 mmol), phenylboronic acid (1.1 mmol) and solvent (3 mL)

^aTetrabutylammonium bromide

^bCetyl trimethyl ammonium bromide

^cSodium dodecylsulfate

^dReaction was performed in the presence of Pd(OAc)₂ as catalyst

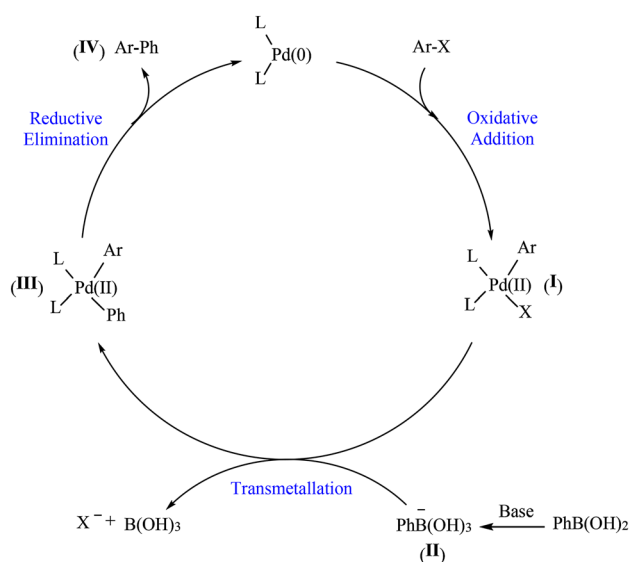
Table 2 Substrate scope for Suzuki–Miyaura cross-coupling reaction using γ -Fe₂O₃/AEPH₂-TC-Pd nanocatalyst

Entry	R ¹	R ²	X	Product	Time (min)	Isolated yield (%)
1	H	H	I	3a	10	98
2	4-NO ₂	H	I	3b	10	98
3	4-Cl	H	I	3c	20	94
4	4-Me	H	I	3d	30	91
5	4-OMe	H	I	3e	55	90
6	2-Me-4-NO ₂	H	I	3f	25	88
7	2-Thiophene	H	I	3g	50	92
8	H	3-NO ₂	I	3h	35	90
9	4-OMe	3-NO ₂	I	3i	55	84
10	H	H	Br	3a	25	95
11	4-NO ₂	H	Br	3b	25	97
12	4-CN	H	Br	3j	25	93
13	4-Cl	H	Br	3c	30	91
14	4-CHO	H	Br	3k	30	89
15	3-CHO	H	Br	3l	45	89
16	4-OMe	H	Br	3e	90	80
17	H	H	Cl	3a	2 h/18 h	20/80
18	4-NO ₂	H	Cl	3b	2 h/18 h	25/82
19	4-CHO	H	Cl	3k	3 h/24 h	20/78
20	4-OMe	H	Cl	3e	3 h/24 h	15/65
21	4-NH ₂	H	Cl	3m	3 h/24 h	0/Trace
22	2-Me-4-NO ₂	H	Cl	3f	2 h/24 h	Trace/30
23	2-Thiophene	H	Cl	3g	5 h/24 h	20/20
24	4-CHO	H	F	3k	24 h	0

Reaction conditions: aryl halide (1 mmol), boronic acid (1.1 mmol), K₂CO₃ (1.2 mmol), TBAB (0.2 mmol), γ -Fe₂O₃/AEPH₂-TC-Pd (0.1 mol%), in H₂O (3 mL) at 40 °C

and *n*-butylamine. This might be due to the well solubility of inorganic bases in the aqueous media. Thus, K₂CO₃ was clearly authenticated as the best option, from the both economic and reaction progress standpoint. By diminishing temperature to 80 °C, the reaction progress became a little sluggish (Table 1, entry 6 vs. 13). During our optimization studies, the effect of using different molar ratios of iodobenzene/K₂CO₃ was also investigated. As observed, by decreasing the amount of K₂CO₃ to 1.2 mmol, the reaction progress was just as good as when the amount of 1.5 mmol was used (Table 1, entry 14). However, no valuable yield of the product was acquired by further reducing the base amount to 1.1 mmol (Table 1, entry 15). On the other hand, upon increasing the amount of K₂CO₃ to 2 mmol, no improvement

was observed in the reaction rate (Table 1, entry 15). In continuation of our efforts to seek more optimal conditions, the effect of catalyst amount was next evaluated. As demonstrated in Table 1, when the desired coupling reaction was conducted in the presence of 0.09 mol% of the nanocatalyst, the product yield was not exceed 82% even after 60 min (Table 1, entry 17). Then, taking advantage of the fact that using a phase-transfer agent would usually promote an organic transformation in aqueous media, the effect of adding 0.2 mmol of tetrabutylammonium bromide (TBAB) to the reaction medium under the previously described conditions was also studied. In this context, the reaction proceeds very surprisingly even at lower temperatures (60 and 40 °C), to furnish a well-yielded product within a short reaction time



Scheme 4 Plausible mechanism for the Suzuki–Miyaura cross-coupling reaction

(Table 1, entries 18–20). Cetyl trimethyl ammonium bromide (CTAB) and sodium dodecylsulfate (SDS) were also examined as phase-transfer agents, but the results represented their less efficiency (Table 1, entries 21, 22). However by decreasing the amount of TBAB, the reaction rate was dropped (Table 1, entry 23). In addition, by keeping other conditions the same, the effect of using Pd(OAc)₂ as catalyst was also investigated. Nevertheless, the result was far from satisfactory in this context (Table 1, entry 24). Ultimately, using 1:1.2 molar ratio of iodobenzene/K₂CO₃ at 40 °C in

the presence of 0.1 mol% of γ -Fe₂O₃/AEPH₂-TC-Pd and 0.2 mmol of TBAB in H₂O was selected as the best optimized condition (Table 1, entry 20).

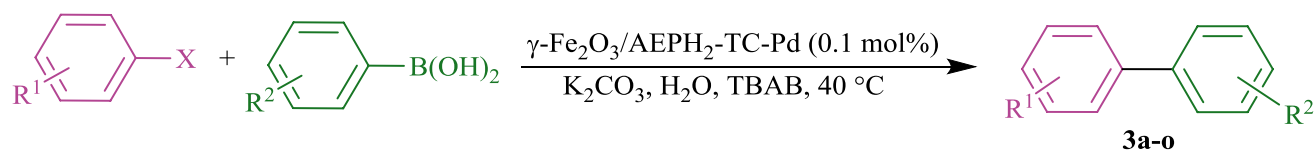
With the optimized reaction conditions in hand, the scope of the Suzuki–Miyaura cross-coupling reaction was extended to various aryl iodides/bromides/chlorides with phenylboronic acids (Table 2). As clearly understood from the results, the designed catalytic system was equally applicable for both aryl iodides and aryl bromides bearing either electron-withdrawing or electron-donating substituents and delivered the corresponding coupled products in good to excellent yields (Table 2, entries 1–16). However, the required times for completion the reactions of related aryl bromides with phenylboronic acids were somewhat longer. Importantly, in a challenging experiment, it was found that the coupling reactions for a number of aryl chlorides with phenylboronic acid were also accompanied with satisfying results, although prolonged times were required due to the stronger strength of carbon-halogen bond in these cases (Table 2, entries 17–20). However, this catalytic system did not support the coupling reactions of phenylboronic acid with some substrates such as 4-chloroaniline, 1-chloro-2-methyl-4-nitrobenzene and 2-chlorothiophene (Table 2, entries 21–23). Also, the reaction of 4-fluorobenzaldehyde with phenylboronic acid was associated with no coupling product (Table 2, entry 24). Interestingly, the prepared catalyst showed improved activity in the Suzuki–Miyaura cross-coupling reaction of highly challenging heterocyclic substrates such as 2-iodothiophene using very low Pd loading (0.1 mol%) to afford the corresponding cross-coupled product in excellent yield (Table 2, entry 7).

Table 3 Heck–Mizoroki cross-coupling reaction of iodobenzene with *n*-butyl acrylate in the presence of γ -Fe₂O₃/AEPH₂-TC-Pd nanocatalyst, under different reaction conditions

Entry	Catalyst (mol%)	Molar ratios of iodobenzene:base	Base	Solvent	Additive (mmol)	Temp. (°C)	Time (min)	Isolated yield (%)
1	0.1	1:1.2	K ₂ CO ₃	H ₂ O	TBAB ^a (0.2)	40	45	79
2	0.1	1:1.2	K ₂ CO ₃	EtOH		40	75	64
3	0.1	1:1.2	K ₂ CO ₃	DMF		40	40	81
5	0.1	1:1.2	K ₂ CO ₃	H ₂ O	TBAB (0.2)	55	35	90
6	0.1	1:1.2	K ₂ CO ₃	H ₂ O	TBAB (0.2)	65	10	98
7	0.1	1:1.2	K ₂ CO ₃	H ₂ O	TBAB (0.2)	90	10	98
8	0.1	1:1.2	K ₂ CO ₃	H ₂ O	TBAB (0.1)	65	45	89
9	0.09	1:1.2	K ₂ CO ₃	H ₂ O	TBAB (0.2)	65	25	73
10	0.2	1:1.2	K ₂ CO ₃	H ₂ O	TBAB (0.2)	65	10	98
11	0.1	1:1.2	Et ₃ N	H ₂ O	TBAB (0.2)	65	35	81
12	0.1	1:1.2	NaHCO ₃	H ₂ O	TBAB (0.2)	65	20	88
13	0.1	1:1.1	K ₂ CO ₃	H ₂ O	TBAB (0.2)	65	20	75
14	–	1:1.2	K ₂ CO ₃	H ₂ O	TBAB (0.2)	65	18 h	15

Reaction conditions: iodobenzene (1 mmol), *n*-butyl acrylate (2 mmol) and solvent (3 mL)

^aTetrabutylammonium bromide

Table 4 Substrate scope for Heck–Mizoroki cross-coupling reaction using γ -Fe₂O₃/AEPH₂-TC-Pd nanocatalyst

Entry	R ¹	R ²	X	Product	Time (min)	Isolated yield (%)
1	H	Bu ⁿ	I	5a	10	98
2	4-NO ₂	Bu ⁿ	I	5b	10	98
3	4-Cl	Bu ⁿ	I	5c	20	95
4	4-Me	Bu ⁿ	I	5d	30	92
5	4-OMe	Bu ⁿ	I	5e	40	91
6	2-Me-4-NO ₂	Bu ⁿ	I	5f	1 h/15 h	Trace/45
7	2-Thiophene	Bu ⁿ	I	5g	55	87
8	H	Me	I	5h	20	96
9	4-NO ₂	Me	I	5i	15	96
10	4-Cl	Me	I	5j	20	92
11	4-Me	Me	I	5k	35	90
12	4-OMe	Me	I	5l	45	90
13	2-Thiophene	Me	I	5m	60	84
14	H	Bu ⁿ	Br	5a	35	89
15	4-NO ₂	Bu ⁿ	Br	5b	35	93
16	4-OMe	Bu ⁿ	Br	5e	60	84
17	H	Me	Br	5h	90	82
18	4-NO ₂	Me	Br	5i	90	91
19	4-CN	Me	Br	5n	90	89
20	4-Cl	Me	Br	5j	90	88
21	4-OMe	Me	Br	5l	120	79
22	H	Me	Cl	5h	2 h/24 h	Trace/79
23	4-NO ₂	Bu ⁿ	Cl	5b	2 h/24 h	20/81
24	4-OMe	Bu ⁿ	Cl	5e	2 h/24 h	Trace/60
25	4-NH ₂	Bu ⁿ	Cl	5o	5 h/24 h	15/15
26	2-Me-4-NO ₂	Bu ⁿ	Cl	5f	4 h/24 h	0/0
27	2-Thiophene	Bu ⁿ	Cl	5g	4 h/24 h	Trace/35

Reaction conditions: aryl halide (1 mmol), acrylate (1.1 mmol), K₂CO₃ (1.2 mmol), TBAB (0.2 mmol), γ -Fe₂O₃/AEPH₂-TC-Pd (0.1 mol%), in H₂O (3 mL) at 65 °C

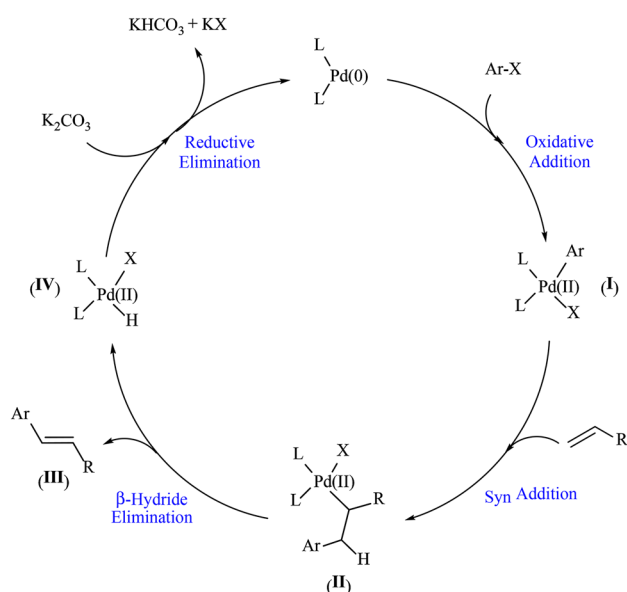
3.4 Proposed Catalytic Mechanism for the Suzuki–Miyaura Cross-Coupling Reaction

By analogy with the previous reports in literature [71], as well as our investigations, the following mechanism can be proposed for the Suzuki–Miyaura cross coupling reaction (Scheme 4). This catalytic pathway involves three sequential steps: oxidative addition, transmetalation and reductive elimination. At first, Pd(0) species undergoes the oxidative addition with aryl halide to deliver the Pd(II) σ -aryl complex (I). Then, in the transmetalation step, the aryl group of the activated arylboronic acid (II) exchanges with the halide on the Pd(II) σ -aryl complex (I) to furnish the Pd(II) diaryl complex (III). Finally, the reductive elimination of III,

facilitates the catalytic cycle by regenerating the active Pd(0) species, while the cross coupled product is produced (IV).

3.5 Catalytic Activity of γ -Fe₂O₃/AEPH₂-TC-Pd in Heck–Mizoroki Cross-Coupling Reaction

Encouraged by the promising results obtained with the Suzuki–Miyaura cross-coupling reaction, the catalytic activity of γ -Fe₂O₃/AEPH₂-TC-Pd nanocatalyst was next explored towards the Heck–Mizoroki cross-coupling reaction (Table 3). At the outset, the model reaction of iodobenzene (1 mmol) with *n*-butyl acrylate (1.1 mmol) was implemented under the optimized conditions for Suzuki–Miyaura reaction. Unfortunately, the result was not as satisfactory as



Scheme 5 Plausible mechanism for the Mizoroki–Heck cross-coupling reaction

expected and the desired product was obtained in only 79% within 45 min (Table 3, entry 1). In an effort to develop more efficient conditions, other solvents such as EtOH and DMF were also examined under the same condition. With regard to the results in Table 3, EtOH was not a pleasing solvent for such a coupling reaction. However, albeit the reaction was speeded up to some extent by using DMF as solvent, its usage was not recommended due to the increasing environmental concerns. To our great delight, significant improvement in the product yield was achieved when the reaction temperature increased to 55 and 65 °C (Table 3, entries 5, 6). More elevated temperatures (90 °C) did not have any positive effect on the reaction progress (Table 3, entry 7). Evaluation of the amount of TBAB and γ -Fe₂O₃/AEPH₂-TC-Pd nanocatalyst clearly documented that the best results were obtained in the presence of 0.2 mmol TBAB and 0.1 mol% nanocatalyst (Table 3, entries 8–10). Less impact of other bases such as Et₃N and NaHCO₃, stipulated that K₂CO₃ is undoubtedly the best one (Table 3, entries 11, 12 vs. entry 6). It is also noteworthy that the molar ratio of iodobenzene:K₂CO₃ has a great influence on this transformation, since the reaction rate declined markedly by decreasing the mentioned ratio (Table 3, entry 13). Notably, a negligible yield of the coupled product was detected in the absence of nanocatalyst, even after 18 h (Table 3, entry 14).

With the optimized conditions in hand, the scope of the γ -Fe₂O₃/AEPH₂-TC-Pd-catalyzed Heck–Mizoroki reactions was investigated by employing various substituted aryl halides to react with *n*-butyl/methyl acrylate (Table 4). Excellent yields of the products were achieved in the coupling reactions of both electron-rich and electron-deficient

aryl iodides with *n*-butyl/methyl acrylates (Table 4, entries 1–13). However, in the case of the electron-releasing aryl iodides, the completion of the reaction is slightly slower. Gratifyingly, the current catalytic system was also effective for the coupling reactions of substituted aryl bromides and also more challenging aryl chlorides, as well. It is worthy of note that the higher the dissociation energies of the C–X bond, the longer the coupling reaction times. Accordingly, the reaction of bromo and chloro derivatives with acrylates needs longer times, respectively, to gain the admissible product yields. Particularly, in the case of the aryl chlorides, the products that were generated at the earliest times of the reactions were unsatisfied.

More importantly, the as-prepared catalyst displayed remarkable activity toward the highly challenging heterocyclic substrates such as 2-iodothiophene and afforded the corresponding products in high yields (Table 4, entries 7 and 13).

During our experiments regarding these coupling transformation, we have met a number of unsuccessful examples which were included in Table 4 to clarify the limitations of the current protocol (Table 4, entries 6 and 25–27). Furthermore, to investigate whether the Heck–Mizoroki reaction was compatible with more diverse substrates, different aryl and heteroaryl olefins such as styrene and 2-vinylpyridine were subjected to react with aryl iodide through the Heck–Mizoroki reaction. The obtained results in these regards were far from satisfactory and poor yields of the coupled products were obtained after 1 h (Yields = 35 and 10% for the reaction of aryl iodide with styrene and 2-vinylpyridine, respectively). However, in the case of the styrene, the product yield was reached to 60% after 24 h, whereas the reaction of the aryl iodide with 2-vinylpyridine did not proceed any more, even after 24 h. These observations demonstrated that the current catalytic system has less efficiency towards the coupling reactions of such substrates (data not given in Table 4).

3.6 Proposed Catalytic Mechanism for the Heck–Mizoroki Cross-Coupling Reaction

According to the literature precedents reports [71], and the results of our researches, a conceivable mechanism for the Heck–Mizoroki cross-coupling reaction is suggested in Scheme 5. Based on the presented mechanism, initially, the active Pd(0) species converts to Pd(II), through the oxidative addition of aryl halide. Thereafter, the syn addition of the resulting palladium intermediate I on olefin compound results to the formation of σ -complex II. In the third step, after the β -hydride elimination, the desired product III is formed. Finally, the reductive elimination by K₂CO₃ on the Pd(II) intermediate IV, provides the Pd(0) species, which can re-enters the catalytic cycle, as well (Scheme 4).

Table 5 Comparison of the catalytic activity of γ -Fe₂O₃/AEPH₂-TC-Pd with some literature precedents for Suzuki–Miyaura and Heck–Mizoroki cross-coupling reactions

Entry	Catalyst (mol%)	Reaction conditions	Time (h)	Yield (%)	References
1 ^a	Fe ₃ O ₄ @SiO ₂ @C22-Pd(II) (0.5)	Et ₃ N, DMF/H ₂ O (1:1), 75 °C	1	92	[72]
2 ^a	Fe ₃ O ₄ @EDTA–PdCl ₂ (20 mg)	K ₂ CO ₃ , TBAB, H ₂ O, 80 °C	3	94	[73]
3 ^a	NHC–Pd(II) complex ^c (0.2)	K ₃ PO ₄ ·3H ₂ O, H ₂ O, TBAB, 40 °C	5	98	[74]
4 ^a	<i>N,N'</i> -bis(2-pyridinecarboxamide)-1,2-benzene palladium complex (1.0)	K ₂ CO ₃ , H ₂ O, 100 °C	3	97	[75]
5 ^a	PdCl ₂ (0.05)	Cs ₂ CO ₃ , DMF, 130 °C	2	95	[76]
6 ^a	PANI–Pd (2.2)	K ₂ CO ₃ , 1,4-dioxane: H ₂ O (1:1), 95 °C	4	91	[77]
7 ^a	Au/Pd NPs (4.0)	K ₂ CO ₃ , EtOH/H ₂ O (2:1), N ₂ atm, 80 °C	24	88	[78]
8 ^a	Pd(II)–NHC complex (0.01 mmol)	Cs ₂ CO ₃ , DMA, 100 °C	24	99	[79]
9 ^a	Pd NPs synthesized by solar irradiation (0.0005 mmol)	KOH, H ₂ O, 100 °C	1	97	[80]
10 ^a	ZrO ₂ @AEPH ₂ -PPh ₂ -Pd(0)	K ₂ CO ₃ , H ₂ O, 80 °C	20	95	[45]
11 ^a	ZrO ₂ @ECP–Pd	K ₂ CO ₃ , H ₂ O, 90 °C	15	98	[52]
12 ^a	γ -Fe ₂ O ₃ /AEPH ₂ -TC-Pd (0.1)	K ₂ CO ₃ , TBAB, H ₂ O, 40 °C	10 min	98	Present work
13 ^b	SMNPs-supported 4,5-diazafuroen-9-one-Pd (0.2)	DABCO, Solvent-free, 140 °C	2	92	[81]
14 ^b	Pd/DIAION HP20 ^d (0.2)	Bu ₃ N, DMA, 100 °C	4	95	[82]
15 ^b	Pd-SMF (1)	Et ₃ N, CH ₃ CN, 100 °C	20	92	[83]
16 ^b	PdCl ₂ (0.02 mmol)	Na ₂ CO ₃ , TBAB, H ₂ O, Ultrasonic Irradiation at 25 °C	4.5	82	[84]
17 ^b	Pd(0)-Arg-boehmite (2.7)	K ₂ CO ₃ , DMF, 120 °C	50 min	98	[71]
18 ^b	MPPI–Pd ^e (0.0007)	Et ₃ N, TBAB, H ₂ O, 100 °C	17	96	[85]
19 ^b	Pd–ZnFe ₂ O ₄ MNPs (4.62)	Et ₃ N, DMF, 120 °C	3	90	[86]
20 ^b	HMMS–NH ₂ –Pd (4)	K ₂ CO ₃ , NMP, 130 °C	8	98	[87]
21 ^b	PdCl ₂ /TiO ₂ (0.5)	Et ₃ N, DMF, under 400 W (mercury vapor lamp) UVvisible irradiation 45 ± 3 °C	5	94*	[88]
22 ^b	ZrO ₂ @ECP–Pd	[bmim]PF ₆ , NEt ₃ , 100 °C	30	95	[52]
23 ^b	ZrO ₂ @AEPH ₂ -sPPh ₂ -Pd(0)	K ₂ CO ₃ , PEG 600, 100 °C	20	95	[45]
24 ^b	γ -Fe ₂ O ₃ /AEPH ₂ -TC-Pd (0.1)	K ₂ CO ₃ , TBAB, H ₂ O, 65 °C	10 min	98	Present work

PANI polyaniline, SMNPs silica-coated magnetite nanoparticles, HMMS monodispersed hollow magnetic spheres

*Conversion

^aSuzuki–Miyaura cross-coupling reaction of iodobenzene with phenylboronic acid

^bHeck–Mizoroki cross-coupling reaction of iodobenzene with *n*-butyl acrylate

^cNHC–Pd(II): [1,1-(hexylene-1,6-diyl)bis(3-*n*-butylbenzimidazol-2-ylidene)][PdCl₂(CH₃CN)]₂

^dDIAION HP20 is a commercial synthetic adsorbent

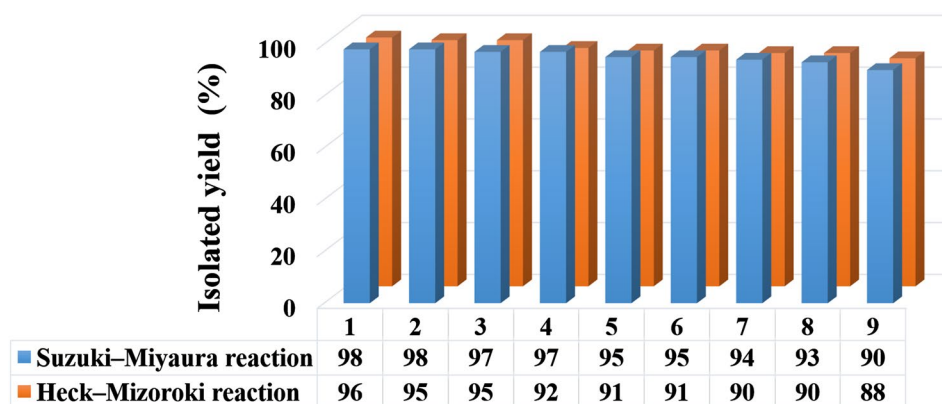
^eConvuluted polymeric palladium catalyst

To further elucidate the merits of the proposed catalytic system over several literature reported catalysts in the Suzuki–Miyaura and Heck–Mizoroki cross-coupling reactions, the comparing efficacy results of some previously reported Pd catalysts against γ -Fe₂O₃/AEPH₂-TC-Pd, was tabulated in Table 5. Even though, each of these catalytic systems has their own advantages, it can be apparently seen that the current catalyst is much superior to almost all of the reported literature precedents not only with respect to the mildness of the reaction conditions, shorter reaction times and reaction high-yields, but also in terms of the convenient catalyst recovery (by using an external magnet), reasonable reusability and high stability.

3.7 Reusability of the γ -Fe₂O₃/AEPH₂-TC-Pd Nanocatalyst

The recycling and recovery of the heterogeneous catalytic systems are very crucial aspects from the economical, industrial and environmental standpoints. In this line, the nanocatalyst reusability was next explored in the model Suzuki–Miyaura and Heck–Mizoroki cross-coupling reactions. At the end of each run, the catalyst was simply separated by an external magnet, washed with ethanol and vacuum-dried at 50 °C to be ready for re-employing directly in another fresh reaction mixture of both catalytic systems. As can be seen in Fig. 9, a negligible decrease in

Fig. 9 Recyclability of $\gamma\text{-Fe}_2\text{O}_3/\text{AEPH}_2\text{-TC-Pd}$ nanocatalyst in the Suzuki–Miyaura and Heck–Mizoroki model reactions, under the optimized conditions



the nanocatalyst activity after successive nine runs, clearly points out that the nanocatalyst was not only very active, but also very stable during the reaction cycles.

The amount of leached Pd into the model Suzuki–Miyaura reaction was also tested, using ICP-OES technique. While, the measured palladium content of the freshly prepared $\gamma\text{-Fe}_2\text{O}_3/\text{AEPH}_2\text{-TC-Pd}$ was estimated to be 0.87 mmol of Pd per 1.00 g of the nanocatalyst, ICP-OES analysis of the 9th recycled catalyst revealed that the recovered nanocatalyst contains 0.85 mmol of Pd per 1.00 g of the nanocatalyst. In the other words, only <1 ppm of the total amount of the original Pd species was lost during the course of the reaction.

Excellent catalytic performance and stability of the aforementioned catalytic system most likely originated from the capability of the sulfur-based ligand for high stabilization of the palladium nanoparticles, which is concerned to the strong interaction of the palladium species and the ligand sulfur atoms [89].

It is noteworthy that the FT-IR spectrum of 9th recovered catalyst (Fig. 1e), revealed the entire preservation of the shape, position and relative intensity of the characteristic absorption bands. These results clearly proved that no substantial changes occurred at the chemical structure of functional groups and the hydrogen bonding network of the designed nanocatalyst.

Furthermore, the XPS spectrum of the 9th recycled $\gamma\text{-Fe}_2\text{O}_3/\text{AEPH}_2\text{-TC-Pd}$ clearly indicated the existence of peaks at 335.1 and 340.3 eV, corresponding to $3d_{5/2}$ and $3d_{3/2}$ for Pd(0) species, respectively (Fig. 3b, d). These findings offered that the oxidation state of the immobilized Pd was preserved even after repeated reactions.

4 Conclusion

In summary, a novel thiophene methanimine–palladium Schiff base complex anchored on $\gamma\text{-Fe}_2\text{O}_3$ functionalized with 2-aminoethyl dihydrogen phosphate ($\gamma\text{-Fe}_2\text{O}_3/\text{AEPH}_2\text{-TC-Pd}$) was designed and fully characterized by different

techniques including FT-IR, XRD, TEM, TGA, ICP-OES, XPS, VSM and elemental analysis. The efficiency of the newly fabricated catalyst was monitored in the aqueous Suzuki–Miyaura and Heck–Mizoroki cross-coupling reactions. Interestingly, the prepared catalytic system displayed improved activity in the cross-coupling reactions of a broad range of aryl iodides, aryl bromides and most importantly the highly challenging aryl chlorides, using very low Pd loading amount. The obtained results based on the hot filtration test, controlled poisoning experiments and ICP-OES analysis clearly confirmed that the respective catalyst operates in a truly heterogeneous manner. This catalyst could be readily recovered (by using a magnetic bar) and reused at least nine times without significant decrease in its catalytic activity. It is worthwhile to mention that the high activity, durability and recyclability of the present catalytic system could be directly attributed to the nature of the applied ligand, which is not only an air and moisture stable ligand intrinsically but also acts as stabilizing Pd NPs agent to protect the palladium species against agglomeration and palladium black formation. Good to excellent yields of the coupled products and short reaction times as well as using H_2O as the reaction media are another advantages that support the current protocol towards the green chemistry.

Acknowledgements The authors gratefully acknowledge the partial support of this study by Ferdowsi University of Mashhad Research Council (Grant No. p/3/39490).

References

1. Simon MO, Li CJ (2012) *Chem Soc Rev* 41:1415
2. Shimizu KI, Satsuma A (2011) *Energy Environ Sci* 4:3140
3. Chen L, Zhang L, Chen Z, Liu H, Luque R, Li Y (2016) *Chem Sci* 7:6015
4. Karami K, Ghasemi M, Haghighat Naeini N (2013) *Catal Commun* 38:10
5. Aghayee M, Zolfigol MA, Keypour H, Yarie M, Mohammadi L (2016) *Appl Organometal Chem* 30:612
6. Colmenares JC, Luque R (2014) *Chem Soc Rev* 43:765

7. Dalaigh CO, Corr SA, Gunko Y, Connon SJ (2007) *Angew Chem Int Ed* 46:4329
8. Liu YH, Deng J, Gao JW, Zhang ZH (2012) *Adv Synth Catal* 354:441
9. Meijere A, Brase S, Oesterich M (2014) *Metal-catalyzed cross coupling reactions and more*. Wiley, Weinheim
10. Horton DA, Bourne GT, Smythe ML (2003) *Chem Rev* 103:893
11. Bringmann G, Gunther C, Ochse M, Schupp O, Tasler S (2001) *Biaryls in nature: a multi-faceted class of stereochemically, biosynthetically, and pharmacologically intriguing secondary metabolites*. Springer, New York
12. Diederich F, Stang PJ (1998) *Metal-catalyzed cross-coupling reactions*. Wiley, New York
13. Luh TY, Leung MK, Wong KT (2000) *Chem Rev* 100:3187
14. Maitlis PM, Haynes A (2006) *Metal-catalysis in industrial organic processes*. RSC Publishing, Cambridge
15. Suzuki A (2011) *Angew Chem Int Ed* 50:6723
16. Negishi EI (2011) *Angew Chem Int Ed* 50:6738
17. Kambe N, Iwasakia T, Terao J (2011) *Chem Soc Rev* 40:4937
18. So CM, Kwong FY (2011) *Chem Soc Rev* 40:4963
19. Herrmann WA, Reisinger CP, Spiegler M (1998) *J Organomet Chem* 557:93
20. Amatore C, Jutand A (1998) *Coord Chem Rev* 178:511
21. Cho JH, Shaughnessy KH (2011) *Synlett* 2011:2963
22. Suzuki A (2003) In: Astruc D (ed) *Modern arene chemistry*. Wiley, Weinheim, pp 53–106
23. Feng XJ, Yan M, Zhang T, Liu Y, Bao M (2010) *Green Chem* 12:1758
24. Ali H, Cauchon N, van Lier JE (2009) *Photochem Photobiol Sci* 8:868
25. Baleizao C, Corma A, Garcia H, Leyva A (2004) *J Org Chem* 69:439
26. Zhang J, Zhao GF, Popovic Z, Lu Y, Liu Y (2010) *Mater Res Bull* 45:1648
27. Xi CJ, Wu YW, Yan XY (2008) *J Organomet Chem* 693:3842
28. Mukherjee A, Sarkar A (2005) *Tetrahedron Lett* 46:15
29. Yang F, Chi C, Dong S, Wang C, Jia X, Ren L, Zhang Y, Zhang L, Li Y (2015) *Catal Today* 256:186
30. Rana S, Maddila S, Yalagala K, Jonnalagadda SB (2015) *Appl Catal A* 505:539
31. Jin X, Zhang K, Sun J, Wang J, Dong Z, Li R (2012) *Catal Commun* 26:199
32. Yan R, Xu JX, Zhang YY, Wang D, Zhang MC, Zhang WQ (2012) *Chem Eng J* 200:559
33. Bohrsch V, Hackenberger CPR (2010) *ChemCatChem* 2:243
34. Yang F, Li YF, Liu T, Xu K, Zhang LQ, Xu CM, Gao JS (2013) *Chem Eng J* 226:52
35. Proch S, Mei Y, Villanueva JMR, Lu Y, Karpov A, Ballauff M, Kempe R (2008) *Adv Synth Catal* 350:493
36. Uozumi Y, Yamada YMA, Beppu T, Fukuyama N, Ueno M, Kitamori T (2006) *J Am Chem Soc* 128:15994
37. Rostamnia S, Nouruzi N, Xin H, Luque R (2015) *Catal Sci Technol* 5:199
38. Perez Y, del Hierro I, Zazo L, Fernandez-Galan R, Fajardo M (2015) *Dalton Trans* 44:4088
39. Doustkhah E, Rostamnia S, Hossieni G, Luque R (2017) *Chem Select* 2:329
40. Rostamnia S, Doustkhah E, Karimi Z, Amini S, Luque R (2015) *ChemCatChem* 7:1678
41. Rostamnia S, Lamei K, Pourhassan F (2014) *RSC Adv* 4:59626
42. Myller AT, Karhe JJ, Pakkanen TT (2010) *Appl Surf Sci* 257:1616
43. Zarghani M, Akhlaghinia B (2015) *RSC Adv* 5:87769
44. Zarghani M, Akhlaghinia B (2015) *Appl Organomet Chem* 29:683
45. Razavi N, Akhlaghinia B, Jahanshahi R (2017) *Catal Lett* 147:360
46. Yousefi Siavashi N, Akhlaghinia B, Zarghani M (2016) *Res Chem Intermed* 42:5789
47. Memar Masjed S, Akhlaghinia B, Zarghani M, Razavi N (2017) *Aust J Chem* 70:33
48. Jahanshahi R, Akhlaghinia B (2017) *New J Chem* 41:7203
49. Jahanshahi R, Akhlaghinia B (2015) *RSC Adv* 5:104087
50. Jahanshahi R, Akhlaghinia B (2016) *RSC Adv* 6:29210
51. Ghodsinia SSE, Akhlaghinia B, Jahanshahi R (2016) *RSC Adv* 6:63613
52. Zarghani M, Akhlaghinia B (2016) *Bull Chem Soc Jpn* 89:1192
53. Jahanshahi R, Akhlaghinia B (2017) *Chem Pap* 71:1351
54. Esmaeilpour M, Akhlaghinia B, Jahanshahi R (2017) *J Chem Sci* 129:313
55. Massart R, Dubois E, Cabuil V, Hasmonay E (1995) *J Magn Magn Mater* 149:1
56. Tucker-Schwartz AK, Garrell RL (2010) *Chem Eur J* 16:12718
57. Sobhani S, Vahidi Z, Zeraatkar Z, Khodadadi S (2015) *RSC Adv* 5:36552
58. Gao Y, Masuda Y, Peng Z, Yonezawa T, Koumoto K (2003) *J Mater Chem* 13:608
59. Klingenberg B, Vannice MA (1996) *Chem Mater* 8:2755
60. Adam F, Hello KM, Osman H (2010) *Chin J Chem* 28:2383
61. Farahani MM, Tayyebi N (2011) *J Mol Catal A* 348:83
62. Sharma RK, Yadav M, Gaur R, Monga Y, Adholecya A (2015) *Catal Sci Technol* 5:2728
63. Svetlichnyi VA, Shabalina AV, Lapin IN (2017) *Russ Phys J* 59:2012
64. Hu J, Sun CF, Gillette E, Gui Z, Wang Y, Lee SB (2016) *Nanoscale* 8:12958
65. Chawla M, Kumar R, Siril PF (2016) *J Mol Catal A* 423:126
66. Li H, Shi L, Sun DE, Li P, Liu Z (2016) *Biosens Bioelectron* 86:791
67. González de Rivera F, Angurell I, Rossell MD, Erni R, Llorca J, Divins NJ, Muller G, Seco M, Rossell O (2013) *Chem Eur J* 19:11963
68. Jiang S, Yi B, Zhao Q, Yu H, Shao Z (2017) *RSC Adv* 7:11719
69. Karimi B, Mansouri F, Mirzaei HM (2015) *ChemCatChem* 7:1736
70. Karimi B, Fadavi Akhavan P (2011) *Inorg Chem* 50:6063
71. Tahmasbi B, Ghorbani-Choghamarani A (2017) *Catal Lett* 147:649
72. Movassagh B, Takallou A, Mobaraki A (2015) *J Mol Catal A* 401:55
73. Azizi K, Ghonchehpour E, Karimi M, Heydari A (2015) *Appl Organomet Chem* 29:187
74. Liu QX, Zhang W, Zhao XJ, Zhao ZX, Shi MC, Wang XG (2013) *Eur J Org Chem* 2013:1253
75. Gholinejad M, Shahsavari HR (2014) *Inorg Chim Acta* 421:433
76. Sabounchei SJ, Hashemi A (2014) *Inorg Chem Commun* 47:123
77. Patel HA, Patel AL, Bedekar AV (2015) *Appl Organomet Chem* 29:1
78. Nasrollahzadeh M, Azarian A, Maham M, Ehsani A (2015) *J Ind Eng Chem* 21:746
79. Xu Q, Duan WL, Lei ZY, Zhu ZB, Shi M (2005) *Tetrahedron* 61:11225
80. Patil AB, Patil DS, Bhanage BM (2012) *J Mol Catal A* 365:146
81. Zolfigol MA, Azadbakht T, Khakyzadeh V, Nejatyami R, Perrin D (2014) *RSC Adv* 4:40036
82. Monguchi Y, Sakai K, Endo K, Fujita Y, Niimura M, Yoshimura M, Mizusaki T, Sawama Y, Sajiki H (2012) *ChemCatChem* 4:546
83. Erathodiyil N, Ooi S, Seayad AM, Han Y, Lee SS, Ying JY (2008) *Chem Eur J* 14:3118
84. Zhang Z, Zha Z, Gan C, Pan C, Zhou Y, Wang Z, Zhou MM (2006) *J Org Chem* 71:4339
85. Sato T, Ohno A, Sarkar SM, Uozumi Y, Yamada Y (2015) *ChemCatChem* 7:2141
86. Singh AS, Patil UB, Nagarkar JM (2013) *Catal Commun* 35:11
87. Wang P, Liu H, Liu M, Li R, Ma J (2014) *New J Chem* 38:1138
88. Waghmode SB, Arbuji SS, Wani BN (2013) *New J Chem* 37:2911
89. Mudd GM (2012) *Platinum Metals Rev.* 56:2